

Position Information-based NOMA for Downlink and Uplink Transmission in Mobile Scenarios

Hao Qiu, Shaoshuai Gao, GuoFang Tu, and Shouxin Zong

Abstract

In this paper, a non-orthogonal multiple access (NOMA) system with partial channel state information (CSI) for downlink and uplink transmission in mobile scenarios is considered, i.e., users are deployed randomly and will move casually around the base station (BS). In this case, the channel gain of each user varies over time, which has an influence on the performance of conventional NOMA. An analytical framework is developed to evaluate the impact of position estimation deviation in terms of decoding order error probability, average sum rate and outage probability. Based on the framework, dynamic power allocation (DPA) for downlink NOMA and dynamic power control (DPC) for uplink NOMA are put forward to optimize the outage performance with user distance information. It has been shown that the performance of NOMA relies on accurate user position information. To this end, two algorithms based on position filtering are proposed to improve the accuracy of user position. Monte Carlo simulation is presented to demonstrate the improvement of spectrum efficiency and outage performance. Simulation results verify the accuracy of the proposed analytical framework.

I. INTRODUCTION

Non-orthogonal multiple access (NOMA) has recently received considerable attention and has been recognized as a promising candidate for future wireless networks [1]. Compared with orthogonal multiple access (OMA), it is considered not only to improve the spectral efficiency but also to support massive connectivity. More users than the number of available orthogonal resource blocks can be supported [2]. The key idea of NOMA is to realize multiple access (MA) by encouraging non-orthogonal resource allocation among users. In particular, NOMA in power domain (PD-NOMA) is inspired by the superposition coding (SC) technology, in which

The authors are with the School of Electronic, Electrical and Communication Engineering, the University of Chinese Academy of Sciences, Beijing 101408, China.

the signals of different users are multiplexed with different power levels. At receivers, successive interference cancellation (SIC) is implemented to decode the superimposed messages [3].

NOMA can be applied into both downlink and uplink transmission. For downlink NOMA, the users with poor channel conditions are usually allocated more power so that their signals are decoded by regarding the signals of others as noise. In [4], the impact of path loss on the performance of NOMA with randomly deployed users was evaluated, which demonstrated that NOMA can outperform conventional OMA. Some works investigated different types of resource allocation, such as user pairing [5] and power allocation [6]. For uplink NOMA, the power control scheme needs to be well-designed so that the base station (BS) is capable of detecting signals from all users. The uplink ergodic sum-rate gain of over OMA was shown in [7]. In [8], a back-off power control scheme was proposed and its outage performance was analyzed. The joint user grouping and power control issue was considered in [9], [10].

The aforementioned literature is under the assumption that both the BS and users can obtain perfect channel information. Actually, this assumption might not be realistic due to many limitations like high mobility of users and channel estimation error. Therefore, some works focused on the case of partial channel state information(CSI) for downlink [11]–[14] and uplink transmission [15], [16]. The impact of channel estimation error on NOMA system was investigated in [11], [12]. In [13], statistical CSI was exploited to optimize the transmit beamforming vectors and the power splitting ratio in the simultaneous wireless information and power transfer (SWIPT)-enabled cooperative NOMA system. In [14], a novel beamforming and cluster strategy was proposed with quantized channel direction information. Moreover, the impact of imperfect CSI on uplink NOMA detection was analyzed in [15]. The authors of [16] evaluated NOMA in a low-latency system and showed that imperfect CSI creates a larger penalty for NOMA than for OMA. For the past several years, some works focused on NOMA with distance information [17]. For instance, distance-based user selection can be adopted in NOMA systems, e.g., [18], [19]. The performance of random beamforming NOMA network with distance information was analyzed in [20]. In [21], the authors verified the rationality of ranking users with distance information for Rayleigh and Nakagami-m fading channels.

There has been massive research on NOMA performance evaluation, and much of them is with the aid of stochastic geometry tools [22]. For instance, the number of users is fixed and they are assumed uniformly distributed within an area, such as [4], [17]. Poisson point process (PPP) or Poisson cluster process (PCP) are also frequently used to model the distribution of transceivers

[18]–[21], [23]. These articles focused on the static scenarios where users are deployed randomly and the locations are independent in different time slots. Recently, the authors of [24] applied NOMA to a visible light communication (VLC) system and the performance was evaluated by using the random walk model. In [25], a machine learning scheme was proposed to demonstrate the NOMA-enabled unmanned aerial vehicles (UAV) placement issue, in which users are roaming on the ground. However, the research of NOMA in mobile scenarios is still limited and more research contribution is required.

Different from previous static NOMA systems like [17], this paper considers a distance-based NOMA system in mobile scenarios, i.e., the users are deployed randomly around the BS and will move casually. It is also different from our previous work [26] since uplink transmission will be considered in this work and a more comprehensive analysis on the effect of position estimation will be presented, including outage performance, user pairing and path loss exponents. Moreover, based on our derived analytical results, two optimization problems are formulated to improve the outage performance in downlink and uplink scenarios. It is noticed that some existing works have studied power optimization problems with distance information, such as power allocation with outage constraints [27], outage balancing [28], ergodic capacity maximization [29] and sum throughput maximization [30]. In this article, the common outage probability (COP) is considered to evaluate the system outage performance. The COP describes the outage performance of the entire NOMA network rather than a single user, which emphasizes the user fairness [31]. To the best of our knowledge, this COP minimization with user distance information has not been considered, and we fill this gap by proposing two dynamic power schemes. The main contributions of this article are summarized as follows:

- We investigate the impact of position estimation error in the distance-based NOMA system. To this end, we adopt a new metric named decoding order error probability to evaluate the effect on user order. The analytical expressions for the average sum rate and outage probability are derived in the two-node pairing case¹. For obtaining more insights, the closed-form approximation of average sum rate at high signal-to-noise ratios (SNR) is provided and indicates that the high-SNR slope is not limited by position estimation error. However, the outage analysis of uplink NOMA shows that an error floor exists when transmission

¹ The results of more users can be extended with the similar method, whereas the process becomes more complex. According to the rationality analysis of NOMA with distance information in [21], $M = 2$ or user pairing is a more practical setting.

power is fixed.

- In order to further improve the outage performance and break the error floor of uplink NOMA, we propose a dynamic power allocation (DPA) scheme for downlink NOMA and a dynamic power control (DPC) scheme for uplink NOMA. More specifically, we optimize the signal power with distance information from the perspective of COP minimization.
- We propose two algorithms based on position filtering to increase the accuracy of position information, which are beneficial to improve the spectrum efficiency and outage performance. In the first algorithm (position tracking-based NOMA), the BS applies a Kalman Filter [32] to track the movement of each user for obtaining more accurate position information. The second algorithm (position prediction-based NOMA) exploits the obtained information of user mobility to predict their positions. It can be applied in the case where frequent position information feedback is unavailable, which strikes a good balance between system performance and network overhead.

The reminder of this paper is organized as follows. Section II describes the system model. In Section III, the impact of position estimation deviation on NOMA average sum rate and outage performance is evaluated, and dynamic signal power schemes are proposed. In Section IV, the position filtering-based NOMA system is designed. Section V provides simulation results and some discussion. Finally, Section VI concludes this paper.

Notations: Matrices and vectors are denoted by upper- and lower-case boldface letters, respectively. The superscript T represents transpose. Expectation is expressed by $E\{\cdot\}$ and probability is described by $\Pr\{\cdot\}$. $\mathcal{N}(\mathbf{a}, \mathbf{R})$ and $\mathcal{CN}(\mathbf{a}, \mathbf{R})$ denote the distribution of real Gaussian random vectors and circularly symmetric complex Gaussian (CSCG) random vectors with mean vector \mathbf{a} , covariance matrix \mathbf{R} , respectively. \mathbf{I}_n is the identity matrix of size n . $\binom{n}{k}$ denotes the binomial coefficient.

II. SYSTEM MODEL

In this paper, we will focus on a single-cell NOMA network in a mobile scenario as shown in Fig. 1. The network consists of one BS and M users U_m ($m = 1, 2, \dots, M$), where the BS and all the users are equipped with a single antenna. It is assumed that the BS is located at the origin of a two-dimensional Euclidean plane, expressed as \mathbb{R}^2 . At the beginning, the users are deployed randomly in the disc D with radius R_D . After that, they are assumed to roam around the BS. The distance between the BS and U_m is denoted by d_m ($m = 1, 2, \dots, M$). For user

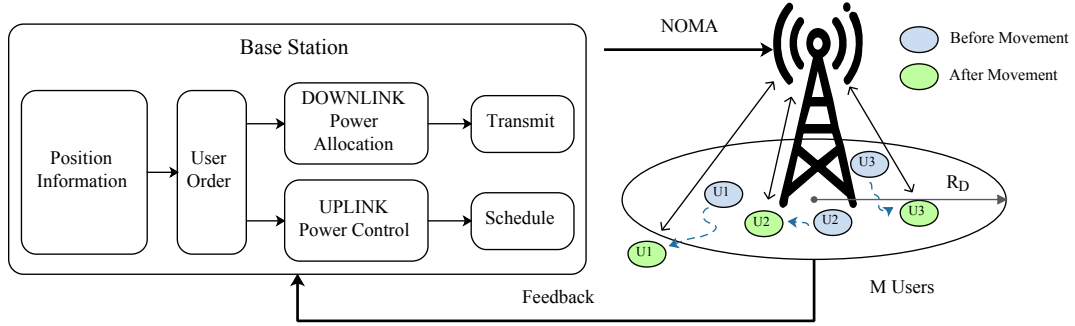


Fig. 1. system model.

position information, positioning of cellular networks can be utilized in the mobile scenario, such as time of arrival (TOA) measurement methods or global positioning system (GPS) [33]. The distance estimation between the BS and users is derived subsequently. Then user order and pairing are determined according to the results as well. We suppose that the position estimation deviation of axis-x and axis-y in the Cartesian coordinate follows a Gaussian distribution with zero mean and variance σ_{ob}^2 for simplicity. In general, the Gaussian distribution assumption is reasonable according to asymptotic arguments and the central limit theorem [34].

On the other hand, wireless channels are assumed to be independent and quasi-static fading, i.e., the channel gain remains constant for a given coherence time and varies independently from one time slot to another. A composite channel model consisting of large-scale path loss and small-scale Rayleigh fading is considered. Thus, the channel coefficient between user U_m and the base station is denoted by $r_m = h_m d_m^{-\alpha/2}$, where $h_m \sim \mathcal{CN}(0, 1)$ and α is the path loss exponent. The channel gain is calculated as $|r_m|^2 = |h_m|^2 d_m^{-\alpha}$, in which $|h_m|^2$ follows an exponential distribution with parameter 1.

A. Downlink NOMA Scheme with Partial Channel Information

In the downlink scenario, the BS transmits messages to the users simultaneously. Without loss of generality, their distances are ranked as $d_1 < d_2 < \dots < d_M$. The signals are superimposed with different power according to the principle of superposition coding. The signal sent by the BS is expressed as follows:

$$S = \sum_{m=1}^M \sqrt{\alpha_m P} S_m, \quad (1)$$

where S_m ($m = 1, 2, \dots, M$) denotes the signal of the user U_m , α_m is its power allocation factor subject to $\sum_{m=1}^M \alpha_m = 1$, and P denotes the transmission power. At receivers, the signal received by user U_m is formulated as

$$y_m = r_m \sum_{l=1}^M \sqrt{\alpha_l P} S_l + n_m, \quad (2)$$

where n_m denotes the Gaussian noise of user U_m . It is normalized with zero mean and variance σ_n^2 , i.e., $n_m \sim \mathcal{CN}(0, \sigma_n^2)$. If SIC is carried out by user U_m , it has to detect the messages of U_l ($m+1 \leq l \leq M$) successfully before detecting its own message. The achievable rate for U_m to detect the signal S_l is shown as follows:

$$R_{m \rightarrow l} = \log_2 \left(1 + \frac{|r_m|^2 \alpha_l}{|r_m|^2 a_{l-1} + \frac{1}{\rho}} \right), \quad (3)$$

where $a_{l-1} = \sum_{k=1}^{l-1} \alpha_k$, $a_0 = 0$, and $\rho = \frac{P}{\sigma_n^2}$ denotes the transmission SNR.

Note that for two users U_i and U_j , we have the following property if $|r_i|^2 > |r_j|^2$:

$$\begin{aligned} R_{i \rightarrow j} &= \log_2 \left(1 + \frac{|r_i|^2 \alpha_j}{|r_i|^2 a_{j-1} + \frac{1}{\rho}} \right) \\ &> \log_2 \left(1 + \frac{|r_j|^2 \alpha_j}{|r_j|^2 a_{j-1} + \frac{1}{\rho}} \right) = R_j. \end{aligned} \quad (4)$$

In other words, the achievable rates are restricted by the users with the poorest channel condition². Moreover, in the delay-tolerant communication, data rates will be determined according to real-time channel conditions and the average sum rate is used as a performance criterion. Assuming that user U_m always decodes the signals S_l ($m+1 \leq l \leq M$) correctly, the sum rate of the system is expressed as follows:

$$R_{sum}^I = \sum_{l=1}^M \min_{1 \leq m \leq l} \log_2 \left(1 + \frac{|r_m|^2 \alpha_l}{|r_m|^2 a_{l-1} + \frac{1}{\rho}} \right). \quad (5)$$

In delay-sensitive communication, messages will be transmitted at a fixed target transmission rate. A typical performance metric is outage probability, which is defined as the probability that the achievable rate under variable channel conditions is less than the target rate. An outage event

² As a special case, the achievable rate of a signal is restricted by themselves only if they are ranked by perfect CSI, such as [4], [5]. However, under the assumption of partial CSI, the property $|r_i|^2 < |r_j|^2$ cannot be guaranteed despite of $d_i < d_j$.

occurs at U_m when S_l ($l \geq m$) fails to be decoded. By denoting the target rate as R_0^* ³, the outage probability of U_m is expressed as

$$P_{om}^I = 1 - \Pr \left\{ \bigcap_{l=m}^M R_{m \rightarrow l} > R_0^* \right\}. \quad (6)$$

We consider the common outage probability (COP) of the network. An outage event occurs if any of the users is in outage. Therefore, the COP is given as follows:

$$P_{cop}^I = 1 - \Pr \left\{ \bigcap_{m=1}^M \bigcap_{l=m}^M R_{m \rightarrow l} > R_0^* \right\}. \quad (7)$$

Some works are based on the assumption that fixed power allocation factors are predetermined no matter which decoding order is selected. Actually, this assumption could lead to poor user fairness or a substantial amount of power is wasted to guarantee the QoS of poor users. To tackle this issue, we will allocate the power to users according to the SIC detection order.

B. Uplink NOMA Scheme with Partial Channel Information

In uplink scenarios, users send signals to the base station at the same time, and they can also be ranked according to distance like downlink. By denoting the transmission power of U_m by P_m , the signal received by the BS is formulated as:

$$y = \sum_{m=1}^M r_m \sqrt{P_m} S_m + n, \quad (8)$$

where n denotes the Gaussian noise. The BS detects the messages by a SIC detector. Unlike downlink, the decoding process starts from the nearest user to the farthest user to make sure that all the signals can be decoded. The achievable rate of the signal S_m is expressed like this:

$$R_m = \log_2 \left(1 + \frac{|r_m|^2 P_m}{\sum_{l=m+1}^M |r_l|^2 P_l + \sigma_n^2} \right). \quad (9)$$

Similar to (5) and (7), the sum rate and outage probability of uplink NOMA are formulated in the following:

$$R_{sum}^{II} = \sum_{m=1}^M R_m = \log_2 \left(1 + \sum_{m=1}^M |r_m|^2 \rho_m \right), \quad (10)$$

$$P_{cop}^{II} = 1 - \Pr \left\{ \bigcap_{m=1}^M R_m > R_0^* \right\}, \quad (11)$$

³ Even though different target rate setting could improve the throughput of the system, the same rate R_0 for the users is assumed in order to guarantee the fairness.

where ρ_m is the transmission SNR of U_m , i.e. $\rho_m = P_m/\sigma_n^2$.

It is worthy to point out that the transmission power of each user is constrained individually. This can be equivalently expressed by largest transmission SNR Ω_m , which means $\rho_m < \Omega_m$.

Note that these metrics are obtained in the case that the optimal channel coding and modulation scheme is adopted. The system considering practical coding and modulation schemes is beyond the scope of this paper, which is likely a promising future direction.

III. PERFORMANCE ANALYSIS AND POWER OPTIMIZATION

In this section, the effect of the position estimation on the system performance is considered. We consider the case when two users are paired for implementation of NOMA like [5]. Without loss of generality, it is assumed that U_1 and U_2 are paired and $d_1 < d_2$. The estimated distance of user U_m is denoted by \hat{d}_m .

A. decoding order error probability

In the distance-based NOMA system, user order may be suboptimal due to channel fading and position estimation error. We adopt a new metric to evaluate their effects on user order, which is named decoding order error probability. It is defined as the probability that the estimated distance-based order is not in accordance with the CSI-based order⁴, which is expressed as

$$P_e = \Pr \left\{ \hat{d}_1 < \hat{d}_2, |r_1|^2 < |r_2|^2 \right\} + \Pr \left\{ \hat{d}_1 > \hat{d}_2, |r_1|^2 > |r_2|^2 \right\}. \quad (12)$$

This metric is used to derive the average sum rate and outage performance later in this section.

Lemma 1. *In the fading-free scenario, the decoding order error probability of distance-based NOMA for the two pairing users with fixed locations is expressed as follows:*

$$P_e^1 = \Pr \left\{ \hat{d}_1 > \hat{d}_2 \right\} = \sum_{i=0}^{\infty} \sum_{j=0}^{\infty} P_{\lambda_1\beta}(i) P_{\lambda_2\beta}(j) I_{i,j}, \quad (13)$$

⁴ Accuracy probability was defined in [21], which means the event when distance-based ranking yields the same results as instantaneous channel information. The decoding order error probability can be regarded as the complementary accuracy probability considering position estimation error. The optimal decoding order has been investigated in [6] and [15].

where $I_{i,j} = \left(\frac{1}{2}\right)^{\alpha_i + \alpha_j} \binom{\alpha_i + \alpha_j - 1}{\alpha_j} F\left(1, \alpha_i + \alpha_j, \alpha_j + 1, \frac{1}{2}\right)$, $\alpha_i = i + 1$, $F(\cdot)$ denotes a hypergeometric function. $P_\lambda(k) = \frac{e^{-\lambda} \lambda^k}{k!}$ ($k \geq 0$) is the probability mass function (PMF) of a Poisson distribution, $\lambda_k = d_k^2$ ($k = 1, 2$), $\beta = \frac{1}{2\sigma_{ob}^2}$.

Proof: Please refer to Appendix A. ■

The lemma indicates that the decoding order error probability is expressed as a weighted sum. The term $I_{i,j}$ is just the function of its indices and the weight coefficients are the probabilities of Poisson distribution. Note that (13) is convergent because P_e^1 is an integral of a joint probability density function as shown in (45). As a result, this probability P_e^1 can be approximated as a sum of finite terms.

In fading-free scenarios, the user order error is only caused by position estimation deviation, and P_e^1 is actually the probability of distance order error. Furthermore, the effect of Rayleigh fading on decoding order error is considered in the following.

Corollary 1. *For the Rayleigh fading channel, the decoding order error probability of distance-based NOMA for the two pairing users with fixed locations is expressed as follows:*

$$P_e^2 = \frac{D-1}{D+1} P_e^1 + \frac{1}{D+1}, \quad (14)$$

where $D = d_2^\alpha / d_1^\alpha$ and the probability P_e^1 has been calculated in Lemma 1.

Proof: We substitute (13) into (12). Due to the independence of channel fading and position estimation, the probability is given by

$$\begin{aligned} P_e^2 &= \Pr(|r_1|^2 > |r_2|^2) \times P_e^1 \\ &\quad + [1 - \Pr(|r_1|^2 > |r_2|^2)] \times (1 - P_e^1). \end{aligned} \quad (15)$$

Let $D = d_2^\alpha / d_1^\alpha$. With some algebraic manipulations, the probability term in (15) is calculated as

$$\Pr(|r_1|^2 > |r_2|^2) = \Pr(|h_2|^2 < D |h_1|^2) = \frac{D}{D+1}. \quad (16)$$

By substituting (16) into (15), this corollary is proved. ■

Given $P_e^1 < 0.5$ and $D > 1$, one can infer from (14) that the error probability is larger than that of the fading-free scenario. The decoding order error event may still occur without positioning deviation due to incomplete CSI. Furthermore, (14) indicates that there is a linear relationship between P_e^1 and P_e^2 . And the impact of decoding order error on the system performance will be investigated with P_e^1 in the following. The conclusions are the same with P_e^2 as well.

B. downlink NOMA system

In downlink transmission, the power is allocated to the two users. Let β denotes the larger power factor, and $1 - \beta$ is for the other.

Proposition 1. *In downlink distance-based NOMA for two pairing users with fixed locations, the average sum rate performance is calculated as follows:*

$$\begin{aligned} R_{sum}^I &= (1 - P_e^1) \varphi'(1, \rho(1 - \beta)) + P_e^1 \varphi'(2, \rho(1 - \beta)) \\ &\quad + \varphi(1, \rho) + \varphi(2, \rho) - \varphi(1, \rho(1 - \beta)) \\ &\quad - \varphi(2, \rho(1 - \beta)), \end{aligned} \quad (17)$$

where $\varphi(k, \phi) = -\frac{\lambda_k}{\lambda \ln 2} e^{\frac{\lambda}{\phi}} \text{Ei}\left(-\frac{\lambda}{\phi}\right)$ and $\varphi'(k, \phi) = -\frac{1}{\ln 2} e^{\frac{\lambda_k}{\phi}} \text{Ei}\left(-\frac{\lambda_k}{\phi}\right)$, $\lambda_k = d_k^\alpha$ ($k = 1, 2$), $\lambda = \lambda_1 + \lambda_2$, $\text{Ei}(x)$ denotes an exponential integral. The probability P_e^1 has been calculated in Lemma 1.

In the high-SNR region, the average sum rate is approximated as

$$R_{sum}^I \approx \log_2 \frac{\rho}{\lambda_1} - P_e^1 \log_2 \frac{\lambda_2}{\lambda_1} - \frac{C}{\ln 2}, \quad (18)$$

where C denotes the Euler's constant [35].

Proof: Please refer to Appendix B. ■

Expressing the function $\varphi'(k, \phi)$ in the form of integral, we have $\varphi'(k, \phi) = \frac{\phi}{\ln 2} \int_0^\infty \frac{e^{-\lambda_k t}}{1+t\phi} dt$. One can see that this function monotonically decreases with λ_k , which indicates $\varphi'(1, \rho(1 - \beta)) > \varphi'(2, \rho(1 - \beta))$ due to $\lambda_1 < \lambda_2$. Therefore, the decoding order error will lead to degradation of the NOMA spectrum efficiency according to (17). The high-SNR approximation shows that the high-SNR slope [12] is not affected by the position deviation and capacity ceilings do not exist.

The optimal power allocation from the perspectives of average sum rate maximization is achieved when all the power is assigned to the near user, i.e., $\beta = 0$, which is also revealed in [29]. Obviously, this strategy is unrealistic and the PA factor should be adjusted considering user fairness constraint. For convenience of analysis, a fixed PA factor is considered in this paper when the average sum rate is analyzed.

Proposition 2. *In downlink distance-based NOMA for two pairing users with fixed locations, let ϵ_0 denotes the target SNR of the two signals, i.e., $\epsilon_0 = 2^{R_0^*} - 1$. The COP is given as follows:*

$$P_{cop}^I = 1 - (1 - P_e^1) e^{-(\lambda_2 A + \lambda_1 \zeta)} - P_e^1 e^{-(\lambda_1 A + \lambda_2 \zeta)}, \quad (19)$$

where $A = \frac{\epsilon_0}{\rho[\beta - (1-\beta)\epsilon_0]}$, $\beta - (1 - \beta) \epsilon_0 > 0$, $B = \frac{\epsilon_0}{\rho(1-\beta)}$, $\zeta = \max\{A, B\}$, and $\lambda_k = d_k^\alpha$ ($k = 1, 2$). The P_e^1 is decoding order error probability from Lemma 1.

Proof: Please refer to Appendix C. ■

An observation is that system parameter setting plays an important role in the outage performance and determines how the positioning deviation affects the COP. Firstly, $\beta > (1 - \beta) \epsilon_0$ needs to be satisfied. Otherwise, the outage probability will always be one. On the condition $A > B$, i.e. $\beta < (1 - \beta) (\epsilon_0 + 1)$, the outage probability is simplified as $P_{cop}^I = 1 - e^{-\lambda A}$. This indicates that positioning deviation has no effect on the COP performance. If $A < B$, i.e. $\beta > (1 - \beta) (\epsilon_0 + 1)$, positioning deviation will lead to the deterioration of the outage performance. When the difference between A and B is large or the difference between λ_1 and λ_2 is large, the impact of estimation deviation will become greater.

In order to improve the outage performance, we propose a dynamic power allocation (DPA) scheme for downlink NOMA based on our analysis above. Our objective is to minimize the COP performance under the total power constraint. Note that the decoding order error probability is a performance metric to evaluate the effect of position estimation, which is unknown to the base station. However, the power allocation can be optimized by using the estimated position information. In this case, even though the approximation is suboptimal, the DPA scheme is practical and effective. We derive its closed-form solution and numerical results in Section V demonstrate the validity. The problem is expressed mathematically as follows:

$$\min_{\beta} 1 - e^{-(\lambda_2 A + \lambda_1 \zeta)}, \quad (20a)$$

$$\text{s.t. } 0 \leq \beta \leq 1, \quad (20b)$$

$$\beta > (1 - \beta) \epsilon_0. \quad (20c)$$

Corollary 2. *The optimal solution to the problem (20) is given by*

$$\beta^* = \frac{\sqrt{1 + \epsilon_0} (\epsilon_0 \lambda_1 - \lambda_2) + \sqrt{\lambda_1 \lambda_2}}{\sqrt{1 + \epsilon_0} [\lambda_1 (1 + \epsilon_0) - \lambda_2]}. \quad (21)$$

Proof: Please refer to Appendix D. ■

C. uplink NOMA system

Different from the downlink NOMA, the average sum rate of uplink is always the same no matter which user is decoded first. The analytical result is given in the following.

Proposition 3. *In uplink distance-based NOMA for two pairing users with fixed locations, the average sum rate is calculated as follows:*

$$R_{sum}^{II} = \left[-\frac{\lambda_1}{\rho_1} \varphi'(2, \rho_2) + \frac{\lambda_2}{\rho_2} \varphi'(1, \rho_1) \right] \times \frac{1}{\frac{\lambda_2}{\rho_2} - \frac{\lambda_1}{\rho_1}}. \quad (22)$$

In the high-SNR region, the approximate average sum rate is expressed as

$$R_{sum}^{II} \approx \left(\frac{\lambda_1}{\rho_1} \log_2 \frac{\lambda_2}{\rho_2} - \frac{\lambda_2}{\rho_2} \log_2 \frac{\lambda_1}{\rho_1} \right) \times \frac{1}{\frac{\lambda_2}{\rho_2} - \frac{\lambda_1}{\rho_1}} - \frac{C}{\ln 2}. \quad (23)$$

Proof: Refer to (10), the average sum rate is written as follows:

$$\mathbb{E}\{C\} = \frac{1}{\rho_1 \rho_2} \iint \log_2(1+x+y) \lambda_1 e^{-\frac{\lambda_1 x}{\rho_1}} \lambda_2 e^{-\frac{\lambda_2 y}{\rho_2}} dx dy. \quad (24)$$

Let $g = \left(\frac{\lambda_1}{\rho_1} + \frac{\lambda_2}{\rho_2} \right) / 2$ and $h = \left(\frac{\lambda_2}{\rho_2} - \frac{\lambda_1}{\rho_1} \right) / 2$. By replacing the integral variables by $t = x + y$ and $s = y - x$, we have

$$\mathbb{E}\{C\} = \frac{g^2 - h^2}{2h} \int_0^\infty \log_2(1+t) e^{-gt} (e^{ht} - e^{-ht}) dt. \quad (25)$$

After substituting (50) and (52) into (25), the exact average sum rate is obtained. Moreover, the high-SNR approximation can be obtained by substituting (56) into (22). ■

Proposition 4. *In uplink distance-based NOMA for two pairing users with fixed locations, the COP is expressed as*

$$P_{cop}^{II} = 1 - (1 - P_e^1) \frac{\lambda_2}{\lambda_2 + k\lambda_1} e^{-\lambda_1 C - (\lambda_2 + k\lambda_1)B} - P_e^1 \times \frac{\lambda_1}{\lambda_1 + k\lambda_2} e^{-\lambda_2 C - (\lambda_1 + k\lambda_2)B}, \quad (26)$$

where $B = \frac{\epsilon_0}{\rho_2}$, $C = \frac{\epsilon_0}{\rho_1}$, $k = \frac{\epsilon_0 \rho_2}{\rho_1}$, and $\lambda_k = d_k^\alpha$ ($k = 1, 2$). P_e^1 is calculated in Lemma 1.

Proof: Please refer to Appendix E. ■

An important observation is that when the transmission power approaches infinity, i.e., $\rho_1 \rightarrow \infty$ and $\rho_2 \rightarrow \infty$, the COP of uplink NOMA is given by

$$P_{cop}^{II} = 1 - (1 - P_e^1) \frac{\lambda_2}{\lambda_2 + k\lambda_1} - P_e^1 \times \frac{\lambda_1}{\lambda_1 + k\lambda_2}. \quad (27)$$

The result shows that the COP is determined by the power ratio of the two users in high SNR region. An error floor exists when transmission power ratio is fixed. This indicates the importance of user power control in uplink NOMA. Based on our analysis, we put forward a dynamic power control scheme (DPC) to break the error floor. After the base station obtains the estimated positions, an optimal transmission power to minimize the COP performance can be found under individual power constraint. Like the downlink PA optimization problem (20), the uplink PC optimization problem is formulated as follows:

$$\min_{\rho_1, \rho_2} 1 - \frac{\lambda_2}{\lambda_2 + k\lambda_1} e^{-\lambda_1 C - (\lambda_2 + k\lambda_1)B}, \quad (28a)$$

$$\text{s.t. } 0 \leq \rho_1 \leq \Omega_1, \quad (28b)$$

$$0 \leq \rho_2 \leq \Omega_2, \quad (28c)$$

where Ω_k is the largest transmission power of user k .

Corollary 3. *The optimal solution to the problem (28) is given by*

$$\rho_1 = \Omega_1, \quad (29a)$$

$$\rho_2 = \min \left(\Omega_2, \frac{\epsilon_0 \lambda_1 \lambda_2 + \lambda_2 \sqrt{4\Omega_1 \lambda_1 + \epsilon_0^2 \lambda_1^2}}{2\lambda_1} \right). \quad (29b)$$

Proof: Please refer to Appendix F. ■

IV. POSITION FILTERING-BASED ALGORITHMS

According to our previous analysis, the SIC strategy relies on accurate position information. Thus in this section, we propose two position filtering-based algorithms, where the movement of users is traceable and this knowledge can be exploited to improve the system performance.

A. User Mobile Model

In this paper, the movement of users is described by a velocity sensor model [34]. This mobility model can be expressed by a continuous-time state-space model. The mobile state of a user is defined by a vector as follows:

$$\mathbf{s}(t) = [x(t), v_x(t), y(t), v_y(t)]^T, \quad (30)$$

where $x(t)$ and $y(t)$ specify the position in the Cartesian coordinate at time t . $v_x(t)$ and $v_y(t)$ denote the velocities in x-axis and y-axis, respectively. Thus, the distance between the user and the base station is calculated as

$$d^2(t) = x^2(t) + y^2(t). \quad (31)$$

Because the velocities change at any time, the variation can be expressed by a white noise stochastic process vector $\mathbf{w}(t)$. Its covariance matrix is denoted by $\tilde{\mathbf{Q}}$.

$$\mathbf{w}(t) = [w_x(t), w_y(t)]^T, \quad \tilde{\mathbf{Q}} = \sigma_w^2 \mathbf{I}_2. \quad (32)$$

The state transition model is expressed with a linear differential equation as

$$\dot{\mathbf{s}}(t) = \tilde{\mathbf{A}}\mathbf{s}(t) + \tilde{\mathbf{B}}\mathbf{w}(t), \quad (33)$$

where $\tilde{\mathbf{A}}$ and $\tilde{\mathbf{B}}$ are state-transition matrix and random input matrix, respectively. They are presented as

$$\tilde{\mathbf{A}} = \begin{bmatrix} 0 & 1 & 0 & 0 \\ 0 & 0 & 0 & 0 \\ 0 & 0 & 0 & 1 \\ 0 & 0 & 0 & 0 \end{bmatrix}, \quad \tilde{\mathbf{B}} = \begin{bmatrix} 1 & 0 \\ 0 & 0 \\ 0 & 1 \\ 0 & 0 \end{bmatrix}. \quad (34)$$

At time t , a measurement of the state vector is made as

$$\mathbf{z}(t) = \mathbf{H}\mathbf{s}(t) + \mathbf{n}_{ob}(t), \quad (35)$$

where \mathbf{H} is the observation matrix and is presented as

$$\mathbf{H} = \begin{bmatrix} 1 & 0 & 0 & 0 \\ 0 & 0 & 1 & 0 \end{bmatrix}, \quad (36)$$

$\mathbf{n}_{ob}(t)$ is the observation noise which is zero mean Gaussian white noise process with covariance matrix $\mathbf{R} = \sigma_{ob}^2 \mathbf{I}_2$

After sampling the state and measurement vector every T seconds, the model is transformed into discrete-time state-space model. Let $\mathbf{s}_k = \mathbf{s}(kT)$ and $\mathbf{z}_k = \mathbf{z}(kT)$, we have

$$\mathbf{s}_{k+1} = \mathbf{A}\mathbf{s}_k + \mathbf{w}_k, \quad (37)$$

where

$$\mathbf{A} = e^{\tilde{\mathbf{A}}T} = \begin{bmatrix} 1 & T & 0 & 0 \\ 0 & 1 & 0 & 0 \\ 0 & 0 & 1 & T \\ 0 & 0 & 0 & 1 \end{bmatrix}, \quad (38)$$

$$\mathbf{w}_k = \int_{kT}^{(k+1)T} e^{\tilde{\mathbf{A}}((k+1)T-\tau)} \tilde{\mathbf{B}} \mathbf{w}(\tau) d\tau, \quad (39)$$

where \mathbf{w}_k is a zero mean discrete-time Gaussian white noise vector, thus $E\{\mathbf{w}_k \mathbf{w}_{k+i}^T\} = 0$ for $i \neq 0$. Besides, the covariance matrix \mathbf{Q} is calculated as

$$\mathbf{Q} = E\{\mathbf{w}_k \mathbf{w}_k^T\} = \begin{bmatrix} T\sigma_w^2 & 0 & 0 & 0 \\ 0 & 0 & 0 & 0 \\ 0 & 0 & T\sigma_w^2 & 0 \\ 0 & 0 & 0 & 0 \end{bmatrix}. \quad (40)$$

Based on this, we propose two algorithms based on position filtering in mobile scenarios.

B. Position tracking-based NOMA

The position tracking-based NOMA carries out position estimation with a Kalman filter, which is based on the principle of minimizing error covariance [32]. The algorithm is divided into two steps as follows:

Step 1: According to the user's state vector, covariance matrix and the observation data, Kalman filter algorithm is performed to obtain the optimal estimated position. Then the distance information is calculated by substituting the result into (31).

Step 2: Users are ranked according to the estimated position and signal power is obtained according to predetermined power scheme. Signals are superimposed at the transmitter for downlink NOMA or they are transmitted simultaneously for uplink NOMA. At receivers, SIC decoding is carried out.

In general, the Kalman filter can be divided into two phases, i.e., prediction and update. In the prediction phase, the estimation of \mathbf{s}_k and its error covariance are denoted by $\hat{\mathbf{s}}_{k|k-1}$ and $\mathbf{P}_{k|k-1}$, respectively. They are denoted by $\hat{\mathbf{s}}_{k|k}$ and $\mathbf{P}_{k|k}$ in the update phase. Let \mathbf{K}_k denotes the Kalman gain. The detailed algorithm procedure is described in Algorithm 1.

Algorithm 1 Position Tracking-Based NOMA

Input: State vector measurement \mathbf{z}_k .

Output: User order and signal power.

Initialization

- 1: Set initial predicted state estimate $\hat{\mathbf{s}}_{1|0} = \mathbf{0}$ and initial predicted error covariance $\mathbf{P}_{1|0} = \mathbf{I}_4$.

Stage 1: Position filtering

- 2: **for** U_i ($i = 1 \dots M$) **do**
- 3: Calculate the Kalman gain:

$$\mathbf{K}_k = \mathbf{P}_{k|k-1} \mathbf{H}^T (\mathbf{H} \mathbf{P}_{k|k-1} \mathbf{H}^T + \mathbf{R})^{-1}.$$
- 4: Updated state equation:

$$\hat{\mathbf{s}}_{k|k} = \hat{\mathbf{s}}_{k|k-1} + \mathbf{K}_k (\mathbf{z}_k - \mathbf{H} \hat{\mathbf{s}}_{k|k-1}).$$
- 5: Updated estimate covariance:

$$\mathbf{P}_{k|k} = (\mathbf{I}_4 - \mathbf{K}_k \mathbf{H}) \mathbf{P}_{k|k-1}.$$
- 6: Calculate the estimated distance: $\hat{d}_k = \hat{x}_k^2 + \hat{y}_k^2$,
 where (\hat{x}_k, \hat{y}_k) is the position coordinate in $\hat{\mathbf{s}}_{k|k}$.
- 7: Predicted state equation: $\hat{\mathbf{s}}_{k+1|k} = \mathbf{A} \hat{\mathbf{s}}_{k|k}$.
- 8: Predicted error covariance: $\mathbf{P}_{k+1|k} = \mathbf{A} \mathbf{P}_{k|k} \mathbf{A}^T + \mathbf{Q}$.
- 9: **end for**

Stage 2: Superposition Coding

- 10: Sort users $\hat{d}_1 \leq \hat{d}_2 \leq \dots \leq \hat{d}_M$.
- 11: User pairing and Scheduling.
- 12: **if** Dynamic power scheme **then**
- 13: Downlink: Calculate PA factor according to (21).
 Uplink: Calculate signal power according to (29).
- 14: **else if** Fixed power scheme **then**
- 15: Downlink: larger PA factor is allocated to far user.
 Uplink: Users transmit signals at maximum individual power constraint.
- 16: **end if**
- 17: Go to Step 2 for the next time slot ($k + 1$).
-

C. Position prediction-based NOMA

Now we consider a more realistic scenario. We know that transmitting the feedback information to the BS may result in a mount of communication overhead and extra transmission delay. In some cases, the position information may be unavailable for some slots. Based on these, we propose the position prediction-based algorithm with less feedback information, while the system performance can also be guaranteed. In the process of position estimation, some knowledge about user mobility is obtained by the BS. This kind of knowledge can be used to predict users' position.

It should be noted that the prediction process is performed at each time slot whether with observation data or not, while the state update process is not needed at the slots without enough observation data. Then the NOMA algorithm is carried out in the same way as the position tracking-based NOMA. The detailed algorithm procedure is shown in Algorithm 2.

Algorithm 2 Position Prediction-Based NOMA

Input: State vector measurement \mathbf{z}_k .

Output: User order and signal power.

Initialization

1: Set initial predicted state estimate $\hat{\mathbf{s}}_{1|0} = \mathbf{0}$ and initial predicted error covariance $\mathbf{P}_{1|0} = \mathbf{I}_4$.

Stage 1: Position filtering

2: **for** U_i ($i = 1 \dots M$) **do**

3: **if** The measurement is available **then**

4: Track the movement of the user the same way as Algorithm 1 (Step 3 to Step 8).

5: **else**

6: Calculate the estimated distance: $\hat{d}_k = \hat{x}_k^2 + \hat{y}_k^2$,
 where (\hat{x}_k, \hat{y}_k) is the position coordinate in $\hat{\mathbf{s}}_{k|k-1}$.

7: Predicted state equation:

$$\hat{\mathbf{s}}_{k+1|k} = \mathbf{A}\hat{\mathbf{s}}_{k|k-1}.$$

8: Predicted error covariance:

$$\mathbf{P}_{k+1|k} = \mathbf{A}\mathbf{P}_{k|k-1}\mathbf{A}^T + \mathbf{Q}.$$

9: **end if**

10: **end for**

Stage 2 is the same as that in Algorithm 1

V. NUMERICAL RESULTS AND DISCUSSIONS

A. simulation results

In this section, numerical results are provided to validate the correctness of our analytical results and evaluate the performance of the proposed NOMA schemes. The parameters used in our simulations are set as follows. The sampling interval is set to $T = 0.2$ s and each sample trajectory includes $K = 300$ sample points, which corresponds to the duration 1 min. Three types of mobility model are considered to mimic the movement of users including random walk model, random waypoint model and Gauss-Markov model [36]. The mobile trajectory of each trial is independent. The small-scale fading is assumed to be Rayleigh fading. The thermal noise

is set as $\sigma_n^2 = -50$ dBm. Monte Carlo simulation results are averaged over 10^6 independent trials.

In terms of OMA benchmark, each user is allocated to one subchannel. The COP is calculated as follows:

$$P_{om}^{III} = 1 - e^{-\frac{\epsilon'_0(\lambda_1 + \lambda_2)}{\rho}}, \quad (41)$$

where ρ denotes the transmission SNR and ϵ'_0 is the target SNR in OMA, i.e., $\epsilon'_0 = 2^{2R_0^*} - 1$.

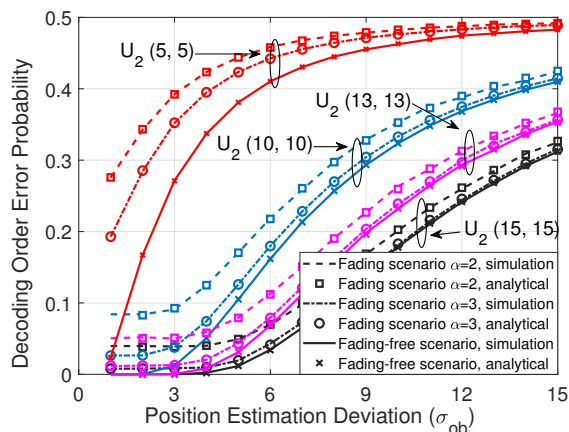


Fig. 2. The decoding order error probability versus position estimation deviation with two users and fixed user position $U_1(3, 3)$.

In Fig. 2, the impact of estimation deviation on the decoding order error probability P_e is investigated. The error probability increases as the position estimation error becomes larger. When users get closer, they are more likely to be disordered. For example, for Rayleigh fading with $\alpha = 3$ and $\sigma_{ob} = 3$, the decoding order error probability is 0.35 for U_2 position (5, 5). When U_2 is at the position (10, 10), the error probability is 0.04. It is worthy to point out that the curves reveal distinct properties under different channel models. For the fading scenario, an error floor can still be observed even with very low deviation. This is because incomplete channel information can lead to an incorrect decision on user decoding order. As we can see, the error probability diminishes with larger path loss exponent α , which is in accordance with the results of [21]. Therefore, the NOMA with partial channel information performs better in high path loss scenarios. The analytical result (13) matches with Monte Carlo simulation.

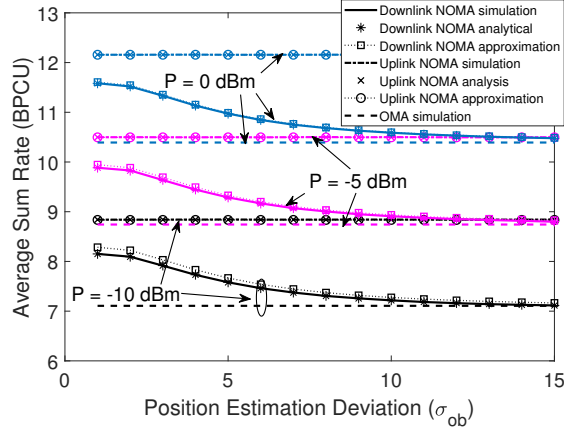


Fig. 3. Impact of position observation noise on NOMA average sum rate (bit per channel use, BPCU) under different transmission power with $M = 2$, $\alpha = 2$, $\beta = 0.8$, and fixed user position $U_1 (3, 3)$, $U_2 (7, 7)$.

In Fig. 3, we demonstrate the influence of position estimation deviation on NOMA average sum rate and compare it with the OMA scheme. As we can see, the average sum rate deteriorates when the observation noise variance σ_{ob}^2 increases. This is because the decoding order error will reduce user rate and cause more detection failure. In accordance to our previous analysis, the average sum rate of uplink is irrelevant to the user order. The comparison with OMA shows that the performance gain of NOMA can still be guaranteed when the estimation error is limited. However, NOMA becomes suboptimal when the positioning deviation is large, which shows the importance of accurate position information.

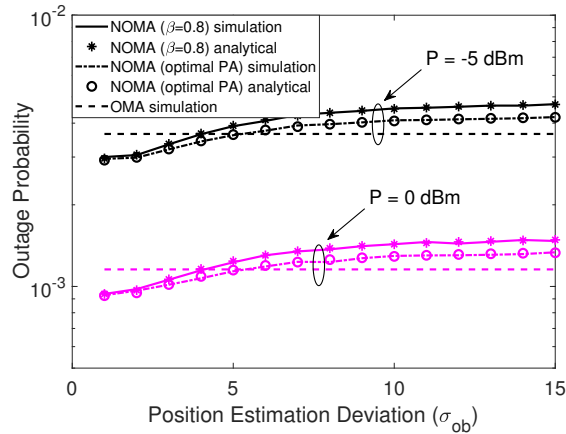


Fig. 4. Impact of position observation noise on downlink outage probability under different transmission power with $M = 2$, $\alpha = 2$, $R_0^* = 0.5$ bit per channel use (BPCU), and fixed user position $U_1 (3, 3)$, $U_2 (7, 7)$.

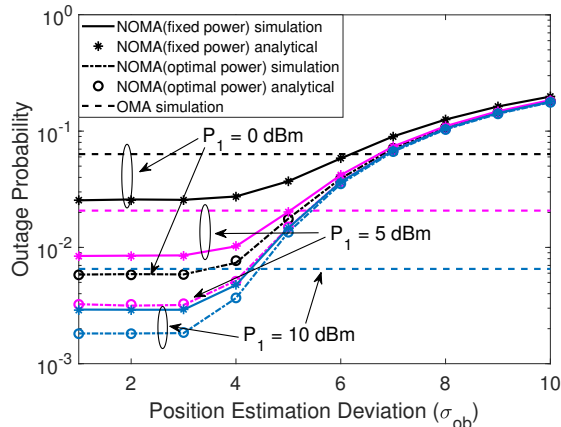


Fig. 5. Impact of position observation noise on uplink outage probability under different transmission power with $M = 2$, $\alpha = 3.5$, $P_2 = 20\text{dBm}$, $R_0^* = 0.1$ BPCU, and fixed user position $U_1(3, 3)$, $U_2(15, 15)$.

The outage performance for downlink and uplink NOMA transmission is shown in Fig. 4 and Fig. 5. The numerical results are in accordance with the Monte Carlo simulation. The results have shown that the proposed dynamic signal power schemes improve their outage performance. However, NOMA may still be worse than OMA when position deviation is high even if the optimal power strategy is adopted. We can observe that compared to downlink, the outage probability of uplink scenario is more sensitive to position deviation. This inspires us to utilize the hybrid NOMA/OMA scheme in uplink transmission. And it also indicates the importance of reducing position estimation error in order to further improve the outage performance.

In order to evaluate the performance in mobile scenarios, three mobility models are considered, i.e., random walk (RW), random waypoint (RWP), and Gauss-Markov model (GM). In random walk model, a user moves to a new location by randomly choosing a direction and speed. Users are allowed to move for an interval before changing their speed and direction. In random waypoint model, users could stay at a location in pause time and then choose the next destination. As for the Gauss-Markov model, the speed and direction are updated at each time slot. The tuning parameter is used to controls the level of randomness. The detailed model parameters are shown in Table I.

Table II illustrates the effectiveness of position filtering because the position deviation decreases for all the three cases, which is beneficial to reduce decoding order error. Taking the GM model as an example and recalling Fig. 2, the decoding order error probability decreases rapidly as σ_{ob} changes from 5 to 2.53, especially when the two users get close. To demonstrate the performance of our scheme, simulation results of spectrum efficiency and outage performance

TABLE I
SIMULATION PARAMETERS OF MOBILITY MODELS

Random Walk (RW)	
Minimum Speed (m/s)	0
Maximum Speed (m/s)	2
Movement Interval (sample points)	30
R_D	30
Random Waypoint (RWP)	
Minimum Speed (m/s)	1
Maximum Speed (m/s)	3
Max Pause Time (sample points)	5
R_D	50
Gauss-Markov Model (GM)	
Speed Variance	2
Tuning Parameter	0.5
R_D	30

TABLE II
COMPARISON OF THREE MOBILITY MODELS

σ_{ob}	RW	RWP	GM
5	2.45	3.45	2.53
$\sqrt{50}$	2.99	4.26	3.09

with GM mobility model are given in the following.

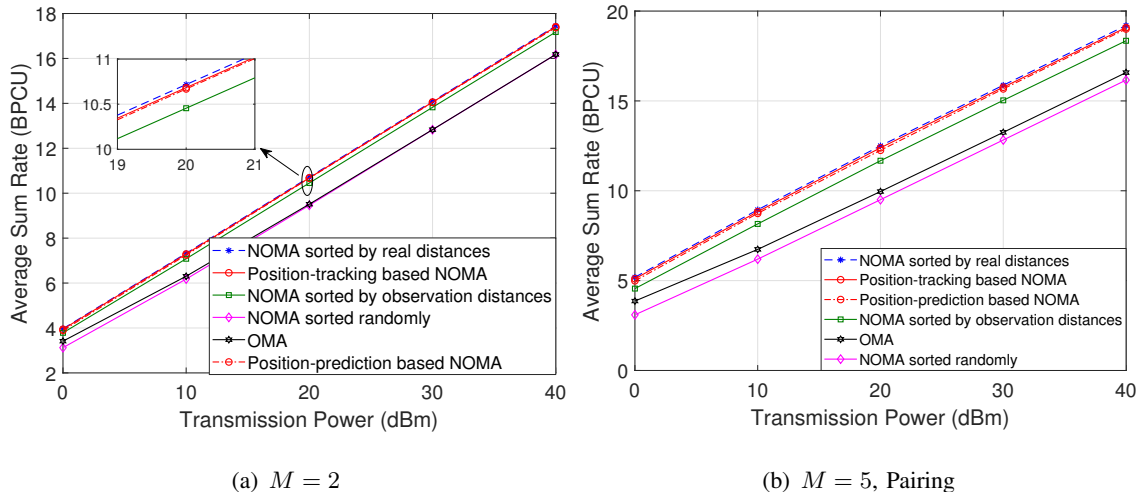


Fig. 6. Average sum rate performance of downlink position filtering-based NOMA with observation noise variance $\sigma_{ob}^2 = 50$ and $\beta = 0.75$.

In Fig. 6, we demonstrate the simulation results for downlink average sum rate performance of our proposed NOMA schemes. As we can see, the curves of the position filtering-based NOMA are close to that with perfect position knowledge, which is the upper bound of distance-based NOMA. For position prediction-based NOMA, the slots in which the BS has access to observation data only account for 25% in our simulation. But the algorithm with incomplete observation data will still obtain an excellent average sum rate performance. User pairing is considered in Fig. 6(b), where the nearest user and farthest user are paired according to the estimated distances. It reveals that the sum rate gap between real distances and observation distances becomes larger compared with Fig. 6(a) where two random users in the network can be paired. This property indicates that position estimation error has a greater influence on the user pairing-based NOMA. Our scheme is more effective when a suitable pairing strategy is adopted due to accurate position estimation.

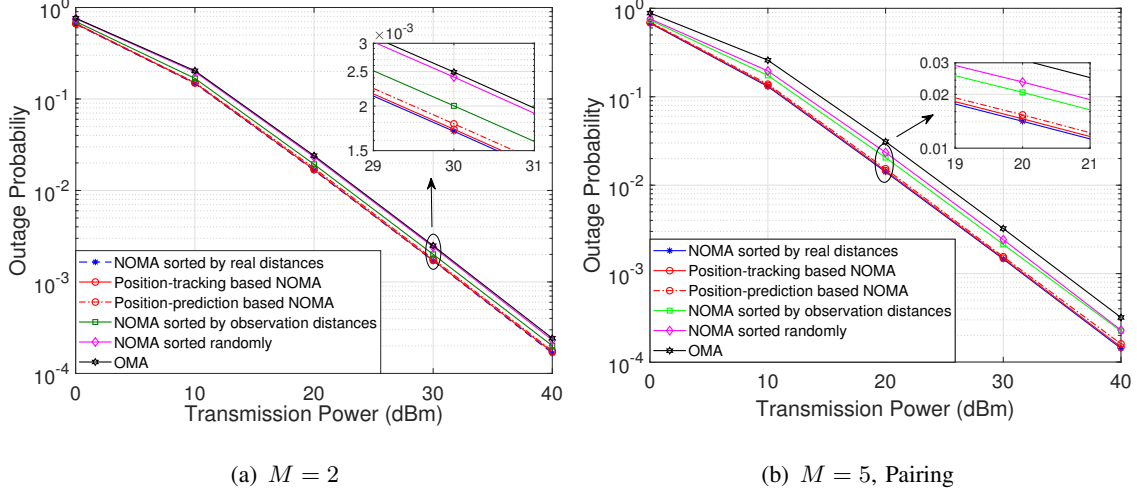


Fig. 7. Outage performance of downlink position filtering-based NOMA with DPA, observation noise variance $\sigma_{ob}^2 = 50$, and target rate $R_0^* = 1.5$ BPCU.

Fig. 7 shows the outage performance simulation results for both pair-based and not pair-based cases. As shown from the figures, our proposed NOMA schemes approach the curves of real distance information. The outage probability of position prediction-based NOMA is almost the same as position tracking-based NOMA even if less position observation is used. As expected, the performance of our scheme is still superior to the OMA.

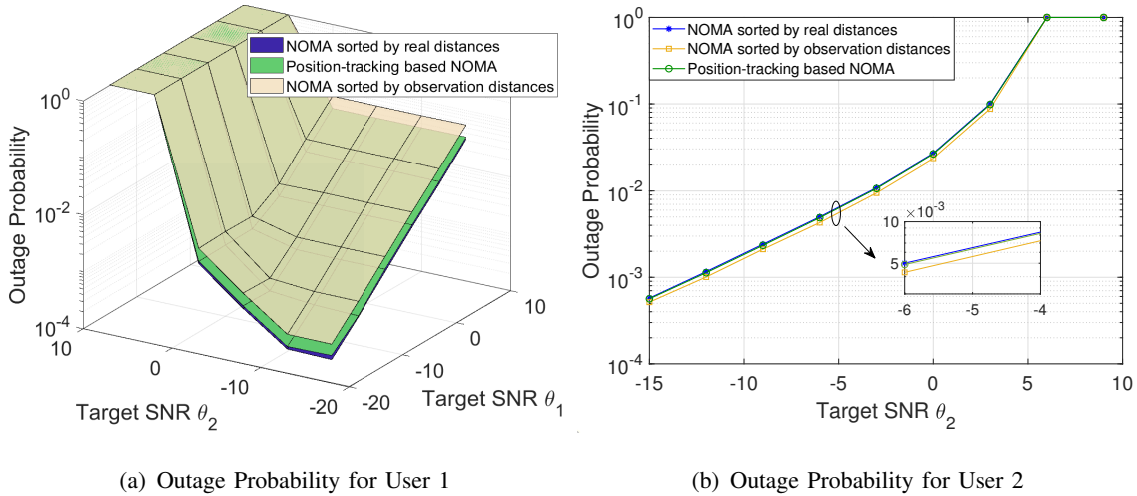


Fig. 8. Outage performance for each user of downlink NOMA versus the target rate of each signal with $\beta = 0.75$, observation noise variance $\sigma_{ob}^2 = 50$ and transmission power $P = 15$ dBm.

Fig. 8 shows the relation between the outage performance of each user and target SNR of each signal in downlink transmission. The target SNR θ_2 affects the outage probability of both two

users, whereas θ_1 has nothing to do with the outage probability for user 1. It can be observed from Fig. 8(a) that the outage performance of position tracking-based NOMA is better than the NOMA sorted by observation distances. Actually, the improvement is at the cost of losing negligible outage performance for user 2 as shown in Fig. 8(b). Furthermore, it is worth pointing out that the choice of target SNR θ_2 also plays a key role in the NOMA with partial CSI. Unsuitable θ_2 will make the outage probability of each user always be one due to the interference-limited property of S_2 .

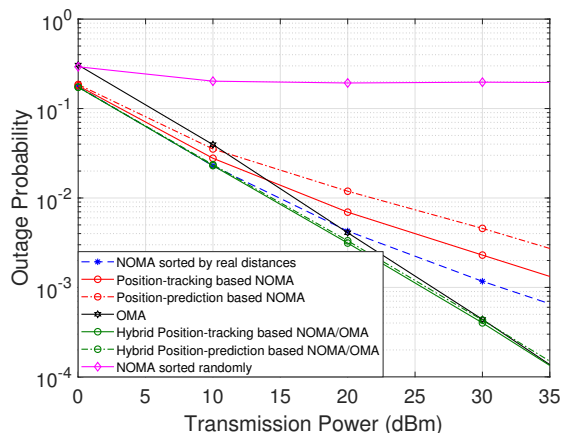


Fig. 9. Outage performance of uplink position filtering-based NOMA with DPC, observation noise variance $\sigma_{ob}^2 = 50$, $\alpha = 3.5$, target rate $R_0^* = 0.1$ BPCU, and $M = 5$ (pairing).

The outage performance of uplink NOMA is given in Fig. 9 when optimal power control strategy is adopted. The error floor does not exist in our scheme. One can be observed that position filtering-based NOMA is a better candidate in the relatively low SNR region, whereas OMA is superior when SNR is high. Thus, to take advantages of the two schemes, a hybrid NOMA/OMA uplink scheme is developed for the practical system. The COP performance is derived firstly according to (26), (41), and the better strategy is chosen adaptively for each uplink transmission. The results of hybrid position filtering-based NOMA/OMA scheme are illustrated in the figure. It can be observed that this hybrid scheme is superior to either single multiuser access protocol.

B. MIMO extension and discussions

The SISO scenario is considered in the previous analysis. Actually, the NOMA scheme can also be combined with MIMO to achieve high spectrum efficiency. The existed MIMO-NOMA

systems can usually be divided into two categories, i.e., multi-cluster NOMA and single-cluster NOMA.

For the first case, each spatial freedom can support a cluster of users and spatial multiplexing is used to remove inter-cluster interference like [37], [38]. Users in the same cluster perform NOMA the same way as SISO-NOMA does. In general, channel gains are highly dependent on beamforming and detection methods, thus the user order is usually determined by channel gain feedback. Especially, when signal alignment is employed among the users in the same cluster [39] or their channels are highly correlative, distance-based user order becomes a reasonable alternative. In this case, the effect of user order is reduced to SISO-NOMA user order problem as analyzed previously.

For the second case, SU-MIMO is extended to multi-user scenarios by superposing signals with different power levels directly [29]. Generally, each user can occupy all the MIMO subchannels and each subchannel is shared by multiple users. In this case, users are usually ranked by distance because their channels are modeled by vectors (or matrix). Similar to the SISO scenario, our proposed position-filtering algorithms will reduce the decoding order error probability due to more accurate position estimation. However, the channel correlation needs to be considered in the MIMO scenarios. The exact closed-form analysis is quite involved and so is the dynamic power scheme. Thus, this work is beyond the scope of this paper and is likely a promising direction.

VI. CONCLUSION

In this paper, we have studied position information-based NOMA in mobile scenarios. The impact of position deviation has been investigated for both downlink and uplink transmission. Dynamic signal power schemes are proposed in order to further improve outage performance. Our analysis has shown that the NOMA superiority over OMA will be reduced due to the position error. Two position filtering-based algorithms have been proposed, i.e., position tracking-based NOMA and position prediction-based NOMA. By comparing our scheme to the conventional NOMA and OMA schemes, the improvement of average sum rate and outage performance is observed from the Monte Carlo simulation.

APPENDIX A
PROOF FOR LEMMA 1

Denote the real position of U_k by (x_k, y_k) and the estimated position by (\hat{x}_k, \hat{y}_k) . Thus the real distance is $d_k^2 = x_k^2 + y_k^2$ and the distance estimation is $\hat{d}_k^2 = \hat{x}_k^2 + \hat{y}_k^2$. Recall that the position deviation is subject to a Gaussian distribution, i.e. $\hat{x}_k \sim \mathcal{N}(x_k, \sigma_{ob}^2)$ and $\hat{y}_k \sim \mathcal{N}(y_k, \sigma_{ob}^2)$. Therefore, \hat{d}_k^2 follows a non-central chi-squared distribution. The probability density function (PDF) is given as follows:

$$f_{\hat{d}_k^2}(x) = \frac{1}{2\sigma_{ob}^2} \exp\left(-\frac{x + \lambda_k}{2\sigma_{ob}^2}\right) I_0\left(\frac{\sqrt{x\lambda_k}}{\sigma_{ob}^2}\right), (x \geq 0), \quad (42)$$

where $\lambda_k = d_k^2$, $I_0(x)$ denotes zero-order modified Bessel function of the first kind. By expressing it in the form of a series and substituting into (42), we have

$$\begin{aligned} f_{\hat{d}_k^2}(x) &= \frac{1}{2\sigma_{ob}^2} \exp\left(-\frac{x + \lambda_k}{2\sigma_{ob}^2}\right) \sum_{i=0}^{\infty} \frac{1}{i! \Gamma(i+1)} \left(\frac{\sqrt{x\lambda_k}}{2\sigma_{ob}^2}\right)^{2i} \\ &= \sum_{i=0}^{\infty} P_{\lambda_k \beta}(i) f_{\alpha_i, \beta}(x), \end{aligned} \quad (43)$$

where $\alpha_i = i + 1$, $\beta = \frac{1}{2\sigma_{ob}^2}$, $P_{\lambda}(k) = \frac{e^{-\lambda} \lambda^k}{k!}$ ($k \geq 0$) is the probability mass function (PMF) of a Poisson distribution, $f_{\alpha, \beta}(x) = \frac{\beta^\alpha x^{\alpha-1} e^{-\beta x}}{\Gamma(\alpha)}$, ($x > 0$) is the PDF of Gamma distribution with parameters α and β . (43) indicates that the PDF of \hat{d}_k^2 is a weighted sum of the Gamma distribution PDF, whose weight coefficients are the probabilities of Poisson distributions. Thus its the cumulative density function (CDF) is calculated naturally as

$$F_{\hat{d}_k^2}(x) = \sum_{i=0}^{\infty} P_{\lambda_k \beta}(i) F_{\alpha_i, \beta}(x), \quad (44)$$

where $F_{\alpha, \beta}(x) = \frac{\gamma(\alpha, \beta x)}{\Gamma(\alpha)}$ is the CDF of Gamma distribution and is expressed as the form of a regularized Gamma function.

In fading-free scenarios, user channel gains are only determined by their path loss. Recall that $d_1 < d_2$, we have $|r_1|^2 > |r_2|^2$. According to (12), the decoding order error event occurs only if the order of distance estimation is incorrect, i.e. $\{\hat{d}_1 > \hat{d}_2\}$. The error probability is formulated as

$$\begin{aligned} P_e^1 &= \Pr\{\hat{d}_1 > \hat{d}_2\} = \Pr\{\hat{d}_1^2 > \hat{d}_2^2\} \\ &= \int_0^{+\infty} \int_0^u f_{\hat{d}_1^2}(u) f_{\hat{d}_2^2}(v) dv du. \end{aligned} \quad (45)$$

TABLE III
RECEIVER DETECTION PROCESS OF RAYLEIGH CHANNELS

	U_1	U_2
$ r_1 ^2 > r_2 ^2, \hat{d}_1 > \hat{d}_2$	S_1	$S_1 \rightarrow S_2$
$ r_1 ^2 < r_2 ^2, \hat{d}_1 < \hat{d}_2$	$S_2 \rightarrow S_1$	S_2
$ r_1 ^2 > r_2 ^2, \hat{d}_1 < \hat{d}_2$	$S_2 \rightarrow S_1$	S_2
$ r_1 ^2 < r_2 ^2, \hat{d}_1 > \hat{d}_2$	S_1	$S_1 \rightarrow S_2$

Substitute (43) to (45), a double integral is obtained. The inner integral result is the CDF of Gamma distribution as shown in (44). After simplification, we obtain the expression shown in (13). The integral term $I_{i,j}$ is calculated as follows:

$$\begin{aligned}
 I_{i,j} &= \int_0^\infty f_{\alpha_i,\beta}(x) F_{\alpha_j,\beta}(x) dx \\
 &\stackrel{(a)}{=} \left(\frac{1}{2}\right)^{\alpha_i+\alpha_j} \binom{\alpha_i+\alpha_j-1}{\alpha_j} F\left(1, \alpha_i+\alpha_j, \alpha_j+1, \frac{1}{2}\right), \tag{46}
 \end{aligned}$$

where the calculation process (a) in (46) is obtained by using the result (6.455) in [35] and $F(\cdot)$ denotes a hypergeometric function. Thus, the proof is completed.

APPENDIX B

PROOF FOR PROPOSITION 1

Recall that the distances of the two users satisfy $d_1 < d_2$ and the results of distance estimation can lead to a different power allocation and detection process. To make it clearer, we show the decoding process and the signals that restrict the achievable rate (marked as boldface) in Table III.

As shown in the table, the detection process is divided into four cases according to distance estimation and the amplitude of fading. Take the first case for example. User U_1 regards the signal S_2 as interference to detect its own message directly. The user U_2 firstly considers its own signal S_2 as interference to detect S_1 and removes S_1 according to SIC strategy, then detects the signal S_2 . So as we can see, the achievable rate of both S_1 and S_2 are limited by U_2 because of its poor channel condition. Let P_k ($k = 1, \dots, 4$) denotes the probability of each case. As a result, the average sum rate is expressed as

$$R_{sum}^I = \sum_{k=1}^4 \mathbb{E}\{C_k\} P_k, \tag{47}$$

where

$$C_1 = \log \left(1 + \frac{|r_2|^2 \beta}{|r_2|^2 (1 - \beta) + \frac{1}{\rho}} \right) + \log (1 + \rho |r_2|^2 (1 - \beta)), \quad (48)$$

and other C_k can be expressed similarly. The key to obtain the average sum rate R_{sum}^I in (47) is to calculate the conditional expectation of each case. Let random variable $X_k = |r_k|^2$ ($k = 1, 2$), and the first expectation term is calculated as follows:

$$\begin{aligned} & \mathbb{E} \left\{ C_1 | X_1 > X_2, \hat{d}_1 > \hat{d}_2 \right\} \\ &= \int_0^\infty \int_{x_2}^\infty C_1(x_2) f(x_1, x_2 | X_1 > X_2) dx_1 dx_2 \\ &= \frac{\lambda_2 \rho}{\lambda \ln 2} \int_0^\infty \frac{e^{-\lambda x_2}}{1 + \rho x_2} dx_2 / \Pr \{ X_1 > X_2 \}. \end{aligned} \quad (49)$$

Recall the following equation

$$\int_0^\infty \frac{e^{-lx}}{1 + x\phi} dx = -\frac{1}{\phi} e^{\frac{l}{\phi}} \text{Ei} \left(-\frac{l}{\phi} \right). \quad (50)$$

Define

$$\varphi(k, \phi) = -\frac{\lambda_k}{\lambda \ln 2} e^{\frac{\lambda}{\phi}} \text{Ei} \left(-\frac{\lambda}{\phi} \right), \quad (51)$$

$$\varphi'(k, \phi) = -\frac{1}{\ln 2} e^{\frac{\lambda_k}{\phi}} \text{Ei} \left(-\frac{\lambda_k}{\phi} \right). \quad (52)$$

By substituting (16), (50) and (51) into (49), we have

$$\mathbb{E} \left\{ C_1 | X_1 > X_2, \hat{d}_1 > \hat{d}_2 \right\} = \varphi(2, \rho) / \left(\frac{D}{D+1} \right). \quad (53)$$

Other terms can be achieved with the similar method. Like (15) and (16), the probability P_k is obtained. By substituting the results into (47), the first part is proved.

When $x < 0$ and $x \rightarrow 0$, the exponential integral can be approximated as

$$\text{Ei}(x) \approx \ln(-x) + C, \quad (54)$$

where C represents the Euler's constant. At high SNRs, i.e., $\phi \rightarrow \infty$, (51) and (52) are approximated by

$$\varphi(k, \phi) \approx -\frac{\lambda_k}{\lambda \ln 2} \left(C + \ln \frac{\lambda}{\phi} \right), \quad (55)$$

$$\varphi'(k, \phi) \approx -\frac{1}{\ln 2} \left(C + \ln \frac{\lambda_k}{\phi} \right). \quad (56)$$

After substituting (55) and (56) into (17), the proof is completed.

APPENDIX C

PROOF FOR PROPOSITION 2

According to Appendix B, the decoding process consists of four cases. Similar to the previous method, we need to analyze each case to formulate the outage performance. The COP can be calculate as $P_{cop}^I = \sum_{k=1}^4 P_{cop}^k P_k$. In accordance to Table III, the outage probability of case 1, i.e., P_{cop}^1 , is expressed like this:

$$P_{cop}^1 = 1 - \Pr \left\{ \frac{X_2 \beta}{X_2 (1 - \beta) + \frac{1}{\rho}} > \epsilon_0, \rho X_2 (1 - \beta) > \epsilon_0 \right. \\ \left. \left| X_1 > X_2, \hat{d}_1 > \hat{d}_2 \right. \right\}. \quad (57)$$

Note that the signal S_1 needs to be decoded by both two users. An outage event will occur to U_1 inevitably if U_2 cannot detect S_1 successfully. The equation (57) is obtained on such a condition. After some mathematical manipulation, we have

$$P_{cop}^1 = 1 - \frac{\Pr \{X_1 > X_2 > \zeta\}}{\Pr \{X_1 > X_2\}}. \quad (58)$$

It is noteworthy that equation (58) is conditioned on $\beta - (1 - \beta) \epsilon_0 > 0$. Otherwise, the outage probability is always equal to one since S_1 can never be decoded successfully. The probability of the numerator is calculated by a double integral and the probability of the denominator has been derived in appendix B. Thus the COP of case 1 is formulated as follows:

$$P_{cop}^1 = 1 - \frac{\lambda_2}{\lambda} e^{-\lambda \zeta} / \left(\frac{D}{D+1} \right). \quad (59)$$

Similarly, the outage probabilities of other cases can be calculated. By substituting the results, the proof is completed.

APPENDIX D

PROOF FOR COROLLARY 2

We can see from Proposition 2 that when $\frac{\epsilon_0}{\epsilon_0+1} < \beta < \frac{\epsilon_0+1}{\epsilon_0+2}$, $P_{cop}^I = 1 - e^{-\frac{\lambda \epsilon_0}{\rho[\beta - (1-\beta)\epsilon_0]}}$. An observation is that the outage probability monotonically decreases with β .

As for the region $\frac{\epsilon_0+1}{\epsilon_0+2} < \beta < 1$, define the function $f(\beta) = \lambda_2 A + \lambda_1 B$. Thus, the monotonicity of P_{cop}^I is determined by $f(\beta)$. The derivative of function with respect to β is calculated as

$$\frac{df}{d\beta} = \frac{\epsilon_0 (a\beta^2 + b\beta + c)}{\rho (1 - \beta)^2 (\beta - \epsilon_0 + \beta\epsilon_0)^2}, \quad (60)$$

where $a = (1 + \epsilon_0) [\lambda_1 (1 + \epsilon_0) - \lambda_2]$, $c = \epsilon_0^2 \lambda_1 - \lambda_2 - \epsilon_0 \lambda_2$, and $b = 2 (1 + \epsilon_0) (\lambda_2 - \epsilon_0 \lambda_1)$. The zero points of (60) exist and are given as follows:

$$\beta^\dagger = \frac{\sqrt{1 + \epsilon_0} (\epsilon_0 \lambda_1 - \lambda_2) \pm \sqrt{\lambda_1 \lambda_2}}{\sqrt{1 + \epsilon_0} [\lambda_1 (1 + \epsilon_0) - \lambda_2]}. \quad (61)$$

Three important features of the roots are shown in the following.

- 1) The root with plus sign β^+ satisfies $\frac{\epsilon_0+1}{\epsilon_0+2} < \beta^+ < 1$. Equivalently, the inequality is expressed as

$$0 < \frac{\lambda_1 \sqrt{1 + \epsilon_0} - \sqrt{\lambda_1 \lambda_2}}{\sqrt{1 + \epsilon_0} [\lambda_1 (1 + \epsilon_0) - \lambda_2]} < \frac{1}{\epsilon_0 + 2}. \quad (62)$$

Namely,

$$0 < \frac{\lambda_1}{\lambda_1 (1 + \epsilon_0) + \sqrt{\lambda_1 \lambda_2} (1 + \epsilon_0)} < \frac{1}{\epsilon_0 + 2}. \quad (63)$$

Recall that $\lambda_1 < \lambda_2$ and all the variables are positive, the inequality (63) is easily proven.

- 2) On the condition of $a > 0$, i.e., $\lambda_1 (1 + \epsilon_0) > \lambda_2$, the root with minus sign satisfies $\beta^- < \frac{\epsilon_0+1}{\epsilon_0+2}$. The result can be proven with similar method above.
- 3) In the case of $a < 0$, $\beta^- > 1$, which is equivalent to

$$\frac{\lambda_1 \sqrt{1 + \epsilon_0} + \sqrt{\lambda_1 \lambda_2}}{\sqrt{1 + \epsilon_0} [\lambda_1 (1 + \epsilon_0) - \lambda_2]} < 0. \quad (64)$$

Note that the numerator is positive and the denominator is negative. Thus its proof has finished.

To sum up, the COP is monotonically decreasing in the region $(\frac{\epsilon_0+1}{\epsilon_0+2}, \beta^+)$ and monotonically increasing in $(\beta^+, 1)$ in either case. Therefore, the proof is completed.

APPENDIX E

PROOF FOR PROPOSITION 4

When $\hat{d}_1 < \hat{d}_2$, the BS decodes S_1 first and S_2 follows. The outage probability at the base station is formulated as

$$\begin{aligned} P_{cop}^1 &= 1 - \Pr \left\{ \frac{\beta X_1}{(1 - \beta) X_2 + \frac{1}{\rho}} > \epsilon_0, \rho (1 - \beta) X_2 > \epsilon_0 \right\} \\ &= 1 - \Pr \{ X_1 > k X_2 + C, X_2 > B \}, \end{aligned} \quad (65)$$

where $B = \frac{\epsilon_0}{\rho_2}$, $C = \frac{\epsilon_0}{\rho_1}$ and $k = \frac{\epsilon_0 \rho_2}{\rho_1}$. The probability in (65) is calculated by the integral of the joint PDF function over the region, which is illustrated as follows:

$$\begin{aligned} p_{cop}^1 &= 1 - \int_B \int_{kX_2+C}^{\infty} \lambda_1 e^{-\lambda_1 X_1} \lambda_2 e^{-\lambda_2 X_2} dX_1 dX_2 \\ &= 1 - \frac{\lambda_2}{\lambda_2 + k\lambda_1} e^{-\lambda_1 C - (\lambda_2 + k\lambda_1)B}. \end{aligned} \quad (66)$$

Similarly, the outage probability of the case $\hat{d}_1 > \hat{d}_2$ can be expressed as follows:

$$P_{cop}^2 = 1 - \frac{\lambda_1}{\lambda_1 + k\lambda_2} e^{-\lambda_2 C - (\lambda_1 + k\lambda_2)B}. \quad (67)$$

Finally, add the weighted results (66) and (67). The result of (26) is obtained.

APPENDIX F

PROOF FOR COROLLARY 3

The transmission power for both users is to be solved. To this end, the problem is separated into two steps, i.e, the transmission SNR of user 1 is firstly optimized for a given ρ_2 . After that, the optimal ρ_2 is calculated for the derived ρ_1 .

Recall that the outage is expressed as

$$P_{cop}^{II} = 1 - \frac{\lambda_2}{\lambda_2 + \frac{\epsilon_0 \lambda_1 \rho_2}{\rho_1}} e^{-\frac{\lambda_1(\epsilon_0 + \epsilon_0^2)}{\rho_1} - \frac{\lambda_2 \epsilon_0}{\rho_2}}. \quad (68)$$

Note that the COP is minimized when U_1 transmits messages at its largest power, which is because a larger transmission power means less outage when the power of the interference signal is constant. Thus, the first part of the proof has finished. By deriving P_{cop}^{II} with respect to ρ_2 , we have

$$\begin{aligned} \frac{dP_{cop}^{II}}{d\rho_2} &= \frac{\Omega_1 \epsilon_0 \lambda_2 e^{-\frac{\lambda_1(\epsilon_0 + \epsilon_0^2)}{\Omega_1} - \frac{\lambda_2 \epsilon_0}{\rho_2}}}{\rho_2^2 (\rho_2 \epsilon_0 \lambda_1 + \Omega_1 \lambda_2)^2} \\ &\quad \times (\lambda_1 \rho_2^2 - \epsilon_0 \lambda_1 \lambda_2 \rho_2 - \Omega_1 \lambda_2^2). \end{aligned} \quad (69)$$

An useful observation is that the fraction in (69) is positive. Therefore, the zero points are given by

$$\rho_2^\dagger = \frac{\epsilon_0 \lambda_1 \lambda_2 \pm \lambda_2 \sqrt{4\Omega_1 \lambda_1 + \epsilon_0^2 \lambda_1^2}}{2\lambda_1}. \quad (70)$$

From (70), it is easy to prove that $\rho_2^\dagger > 0$ and $\rho_2^- < 0$. According to the monotonicity similar to Appendix D, the optimal transmission SNR for U_2 is obtained.

$$\rho_2^* = \min(\Omega_2, \rho_2^\dagger). \quad (71)$$

REFERENCES

- [1] L. Dai, B. Wang, Z. Ding, Z. Wang, S. Chen, and L. Hanzo, "A survey of non-orthogonal multiple access for 5G," *IEEE Commun. Surveys Tuts.*, vol. 20, no. 3, pp. 22942323, 3rd Quart., 2018.
- [2] Y. Saito, A. Benjebbour, Y. Kishiyama, and T. Nakamura, "Systemlevel performance evaluation of downlink non-orthogonal multiple access (NOMA)," in *Proc. IEEE Int. Symp. Pers., Indoor Mobile Radio Commun. (PIMRC)*, Sep. 2013, pp. 611615.
- [3] S. M. R. Islam, N. Avazov, O. A. Dobre and K. Kwak, "Power-domain non-orthogonal multiple access (NOMA) in 5G systems: Potentials and challenges," *IEEE Commun. Surveys Tuts.*, vol. 19, no. 2, pp. 721742, 2nd Quart., 2017.
- [4] Z. Ding, Z. Yang, P. Fan, and H. V. Poor, "On the performance of non-orthogonal multiple access in 5G systems with randomly deployed users," *IEEE Signal Process. Lett.*, vol. 21, no. 12, pp. 15011505, Dec. 2014.
- [5] Z. Ding, P. Fan, and H. V. Poor, "Impact of user pairing on 5G nonorthogonal multiple-access downlink transmissions," *IEEE Trans. Veh. Technol.*, vol. 65, no. 8, pp. 60106023, Aug. 2016.
- [6] Z. Yang, W. Xu, C. Pan, Y. Pan, and M. Chen, "On the optimality of power allocation for NOMA downlinks with individual QoS constraints," *IEEE Commun. Lett.*, vol. 21, no. 7, pp. 16491652, July 2017.
- [7] Z. Wei, L. Yang, D. W. K. Ng, J. Yuan, and L. Hanzo, "On the performance gain of NOMA over OMA in uplink communication systems," *IEEE Trans. Commun.*, vol. 68, no. 1, pp. 536-568, Jan. 2020.
- [8] N. Zhang, J. Wang, G. Kang, and Y. Liu, "Uplink nonorthogonal multiple access in 5G systems," *IEEE Commun. Lett.*, vol. 20, no. 3, pp. 458461, Mar. 2016.
- [9] Z. Yang, Z. Ding, P. Fan, and N. Al-Dhahir, "A general power allocation scheme to guarantee quality of service in downlink and uplink NOMA systems," *IEEE Trans. Wireless Commun.*, vol. 15, no. 11, pp. 72447257, Nov. 2016.
- [10] M. S. Ali, H. Tabassum, and E. Hossain, "Dynamic user clustering and power allocation for uplink and downlink non-orthogonal multiple access (NOMA) systems," *IEEE Access*, vol. 4, pp. 63256343, 2016.
- [11] S. Arzykulov, G. Nauryzbayev, T. A. Tsiftsis, B. Maham, and M. Abdallah, "On the outage of underlay CR-NOMA networks with detect-and-forward relaying," *IEEE Trans. Cogn. Commun. Netw.*, vol. 5, no. 3, pp. 795-804, Sep. 2019.
- [12] X. Li, J. Li, Y. Liu, Z. Ding, and A. Nallanathan, "Residual transceiver hardware impairments on cooperative NOMA networks," *IEEE Trans. Wireless Commun.*, vol. 19, no. 1, pp. 680-695, Jan. 2020.
- [13] J. Liu, K. Xiong, Y. Lu, P. Fan, Z. Zhong, and K. B. Letaief, "SWIPT-enabled full-duplex NOMA networks with full and partial CSI," *IEEE Trans. Green Commun. Netw.*, [early access].
- [14] M. M. Al-Wani, A. Sali, N. K. Noordin, S. J. Hashim, C. Y. Leow, and I. Krikidis, "Robust beamforming and user clustering for guaranteed fairness in downlink NOMA with partial feedback," *IEEE Access*, vol. 7, pp. 121599-121611, 2019.
- [15] Y. Gao, B. Xia, Y. Liu, Y. Yao, K. Xiao, and G. Lu, "Analysis of the dynamic ordered decoding for uplink NOMA systems with imperfect CSI," *IEEE Trans. Veh. Technol.*, vol. 67, no. 7, pp. 66476651, July 2018.
- [16] S. Schiessl, M. Skoglund, and J. Gross, "NOMA in the uplink: Delay analysis with imperfect CSI and finite-length coding," *IEEE Trans. Wireless Commun.*, [early access].
- [17] Z. Yang, Z. Ding, P. Fan, and G. K. Karagiannidis, "On the performance of non-orthogonal multiple access systems with partial channel information," *IEEE Trans. Commun.*, vol. 64, no. 2, pp. 654667, Feb. 2016.
- [18] Y. Liu, Z. Ding, M. Elkashlan, and H. V. Poor, "Cooperative non-orthogonal multiple access with simultaneous wireless information and power transfer," *IEEE J. Sel. Areas Commun.*, vol. 34, no. 4, pp. 938953, Apr. 2016.
- [19] Z. Ding, R. Schober, and H. V. Poor, "A general MIMO framework for NOMA downlink and uplink transmission based on signal alignment," *IEEE Trans. Wireless Commun.*, vol. 15, no. 6, pp. 44384454, June 2016.

- [20] Z. Ding, P. Fan, and H. V. Poor, "Random beamforming in millimeter-wave NOMA networks," *IEEE Access*, vol. 5, pp. 7667-7681, 2017.
- [21] M. Salehi, H. Tabassum, and E. Hossain, "Accuracy of distance-based ranking of users in the analysis of NOMA systems," *IEEE Trans. Commun.*, vol. 67, no. 7, pp. 5069-5083, July 2019.
- [22] M. Haenggi, *Stochastic Geometry for Wireless Networks*. Cambridge, U.K.: Cambridge Univ. Press, 2012.
- [23] Z. Ding, P. Fan, G. K. Karagiannidis, R. Schober, and H. V. Poor, "NOMA assisted wireless caching: Strategies and performance analysis," *IEEE Trans. Commun.*, vol. 66, no. 10, pp. 48544876, Oct. 2018.
- [24] H. Marshoud, V. M. Kapinas, G. K. Karagiannidis, and S. Muhaidat, "Non-orthogonal multiple access for visible light communications," *IEEE Photon. Technol. Lett.*, vol. 28, no. 1, pp. 5154, Jan. 1, 2016.
- [25] Y. Liu, Z. Qin, Y. Cai, Y. Gao, G. Y. Li, and A. Nallanathan, "UAV communications based on non-orthogonal multiple access," *IEEE Wireless Commun.*, vol. 26, no. 1, pp. 5257, Feb. 2019.
- [26] H. Qiu, S. Gao, G. Tu, and S. Zong, "Position filtering-based non-orthogonal multiple access in mobile scenarios," in *Proc. IEEE Int. Conf. Commun. (ICC)*, May 2019, pp. 16.
- [27] J. Cui, Z. Ding, and P. Fan, "A novel power allocation scheme under outage constraints in NOMA systems," *IEEE Signal Process. Lett.*, vol. 23, no. 9, pp. 1226-1230, Sep. 2016.
- [28] S. Shi, L. Yang, and H. Zhu, "Outage balancing in downlink nonorthogonal multiple access with statistical channel state information," *IEEE Trans. Wireless Commun.*, vol. 15, no. 7, pp. 4718-4731, July 2016.
- [29] Q. Sun, S. Han, C. I, and Z. Pan, "On the ergodic capacity of MIMO NOMA systems," *IEEE Wireless Commun. Lett.*, vol. 4, no. 4, pp. 405408, Aug. 2015.
- [30] X. Wang, J. Wang, L. He, and J. Song, "Outage analysis for downlink NOMA with statistical channel state information," *IEEE Wireless Commun. Lett.*, vol. 7, no. 2, pp. 142-145, April 2018.
- [31] P. Xu, Y. Yuan, Z. Ding, X. Dai, and R. Schober, "On the outage performance of non-orthogonal multiple access with 1-bit feedback," *IEEE Trans. Wireless Commun.*, vol. 15, no. 10, pp. 6716-6730, Oct. 2016.
- [32] R. E. Kalman, "A new approach to linear filtering and prediction problems," *Trans. ASME, D, J. Basic Eng.*, vol. 82, pp. 3545, 1960.
- [33] S. M. Razavi et al., "Positioning in cellular networks: Past, present, future," in *Proc. IEEE Wireless Commun. Netw. Conf. (WCNC)*, Apr. 2018, pp. 1-6.
- [34] F. Gustafsson, and F. Gunnarsson, "Mobile positioning using wireless networks: Possibilities and fundamental limitations based on available wireless network measurements," *IEEE Signal Process. Mag.*, vol. 22, no. 4, pp. 4153, July 2005.
- [35] I. S. Gradshteyn, and I. M. Ryzhik, *Table of Integrals, Series, and Products*, 6th ed. New York, NY, USA: Academic, 2000.
- [36] T. Camp, J. Boleng, and V. Davies, "A survey of mobility models for ad hoc network research," *Wireless Commun. Mobile Comput.*, vol. 2, no. 5, pp. 483502, Sep. 2002.
- [37] Z. Ding, F. Adachi, and H. V. Poor, "The application of MIMO to non-orthogonal multiple access," *IEEE Trans. Wireless Commun.*, vol. 15, no. 1, pp. 537552, Jan. 2016.
- [38] M. Zeng, W. Hao, O. A. Dobre, and H. V. Poor, "Energy-efficient power allocation in uplink mmWave massive MIMO with NOMA," *IEEE Trans. Veh. Technol.*, vol. 68, no. 3, pp. 3000-3004, March 2019.
- [39] Z. Ding, R. Schober, and H. V. Poor, "A general MIMO framework for NOMA downlink and uplink transmission based on signal alignment," *IEEE Trans. Wireless Commun.*, vol. 15, no. 6, pp. 44384454, June 2016.